POLITECNICO DI TORINO
Repository ISTITUZIONALE

Optimal design of IPM-PMASR motors for wide constant power speed range applications

Original
Optimal design of IPM-PMASR motors for wide constant power speed range applications / Vagati, Alfredo; Guglielmi, Paolo; Pellegrino, GIAN - MARIO LUIGI; Armando, Eric Giacomo. - 1:(2007), pp. 1-6. (Intervento presentato al convegno PCIM - Power Conversion and Intelligent Motion tenutosi a Norimberga (Germania) nel 21-24 MAY 2007).

Availability:
This version is available at: 11583/1637495 since:

Publisher:
Mesago

Published
DOI:

Terms of use:

This article is made available under terms and conditions as specified in the corresponding bibliographic description in the repository

Publisher copyright

(Article begins on next page)

12 October 2024

Optimal Design of IPM-PMASR motors for wide constant power speed range applications

P. Guglielmi, E. Armando, G.M. Pellegrino, A.Vagati.
Dipartimento di Ingegneria Elettrica - Politecnico di Torino
Corso Duca degli Abruzzi, 24 Torino, 10129 ITALY

***Abstract*— The design of an IPM-PMASR machine represents a trade off between the magnet quantity and the realization of a high anisotropic rotor structure. The better the obtained anisotropy is, the lower the required magnet quantity is. The magnet addition always affects in a positive manner both power factor and machine torque. However, when a large CPSR is required, a low magnet quantity also allows a safe operation at high speed, where a sudden overvoltage could appear in case of inverter fault. For this reason, the rotor anisotropy has to be maximized.**

I. INTRODUCTION

A large interest is nowadays devoted to Interior Permanent Magnet (IPM) motors, because of the many advantages against the competitor a.c. drives, markedly the induction motor drives. In addition to the high efficiency and high torque-density which are typical of PM machines, IPM motors exhibit inherent suitability to zero-speed sensorless control (because of the anisotropic nature) and also can show very good constant-power speed ranges (CPSR), if they are suitably designed at that aim. We can mention, as typical applications: spindle drives, drives for electric and hybrid vehicles, domestic washing machines, etc. In the literature, the design problem has been discussed by many papers [1], [2], [6]–[8], [10]. In spite of that, the design approach is far from standardized, particularly when a large CPSR is wanted. In this paper an exhaustive design procedure is illustrated, starting on previous papers [2]–[5], [9] and aiming to optimized design of IPM motors suited to large CPSRs, called IPM-PMASR motors in the following.

II. IPM-PMASR MOTORS AND CPSR

In general, IPM motors show both PM and reluctance torques, because of their anisotropic rotor. Consequently, PM and reluctance fluxes can be pointed-out, the latter being produced by stator current. Reference is made to eq.(1). Since iron saturation limits the amplitude λ of the total flux vector and the inverter ratings limit the amplitude i of the current vector, the share between λ_m and λ_r becomes a design variable, provided that the physical constraints are satisfied.

$$\lambda_{dq} = \lambda_{mdq} + \lambda_{rdq} \qquad ; \qquad \lambda_{rdq} = L_{dq} i_{dq} \tag{1}$$

An IPM machine whose reluctance torque and flux prevail with respect to PM ones can be called a Permanent Magnet Assisted Synchronous Reluctance (PMASR) machine. Of course, in this case a large anisotropy ratio is needed, to produce the expected torque amount. For PMASR motors the synchronous (d,q) frame is preferably chosen with the d-axis aligned to the direction of maximum permeance, as usual for Synchronous Reluctance (SyR) motors. As a consequence, the PM flux results in -q direction. The anisotropy ratio is defined as $\zeta = Ld/Lq >> 1$. The torque is given by eq.(2).

$$T = \frac{3}{2}\, p\big[\lambda_m\, i_d + (L_d - L_q)\, i_d\, i_q\big] \tag{2}$$

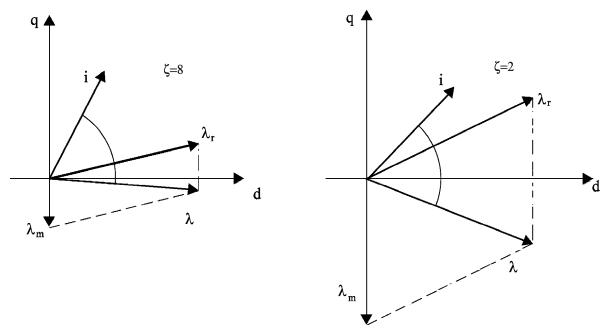

Fig. 1. Examples of IPM and IPM-PMASR (left) vector diagrams.

As can be seen from Fig.1, the left diagram refers to a PMASR motor, while the right one does not. Both diagrams can give the same torque, but the PM contribution is quite different. Coming now to CPSR and flux weakening capability, every IPM machine must satisfy condition (3), firstly stated by Shiferl and Lipo [1].If the (rated) current vector i_0 is rotated towards the q-axis, the total flux vector (moving on an ellipse, depending on ζ) must reach the origin. In this way, a virtually infinite CPSR is obtained, at load.

$$\lambda_q\, i_0 = \lambda_m \tag{3}$$

Let us observe that condition (3) can be satisfied for both IPM and PMASR machines, by proper tailoring λ_m and/or i_0 values. However, eq.(3) is a necessary but not sufficient condition, for a large CPSR performance. In fact, at no-load and high speed, demagnetizing i_q components are needed, when the minimum wanted flux λ_{min} is lower than λ_m. In addition, a worse problem is represented by the Uncontrolled Generator Operation (U.G.O.) which can arise at high speed in case of inverter failure, when $\lambda_m > \lambda_{min}$. The motor e.m.f. suddenly jumps to quite large values and the DC bus capacitance is charged up, through the inverter's diodes.

Additional protection circuitry may be provided, in this case. Anyway, a limit to λ_m/λ_{min} has to be fixed by machine design. As a consequence, the amplitude ω_{max}/ω_b of the CPSR becomes inversely proportional to λ_m.

This point is of particular relevance, because it states that only a PMASR design can be suited to large CPSRs. In other words, the λ_m flux must be as low as possible, which implies that the rotor anisotropy has to be maximized. On the contrary, an IPM machine with a large PM flux component shows an inherently limited CPRS, in practice.

From eq.(2), eq.(4) is easily obtained, by introducing the flux amplitude λ and its argument δ, with respect to d-axis. At high speed the voltage amplitude is limited to V_s. Since $\omega\lambda \simeq V_s$, eq.(4) also show the torque behaviour when the voltage saturation occurs. By taking the partial derivative with respect to δ eq.(5) is obtained, as defining the δ_0 value for which the maximum torque is reached, at fixed voltage.

$$T = \frac{3}{2}\, p\big[\big(\frac{1}{L_q} - \frac{1}{L_d}\big)\lambda^2 \,\sin\delta\cos\delta + \frac{\lambda_m}{L_q}\lambda\,\cos\delta\big] \quad (4)$$

$$2\sin^2\delta_0 + \alpha\sin\delta_0 - 1 = 0 \qquad ; \qquad \alpha = \frac{\lambda_m}{\lambda}\cdot\frac{\zeta}{\zeta - 1} \quad (5)$$

From eq.(5) the unique solution (6) is obtained. The parameter α practically coincides with λ_m/λ, being $\zeta >> 1$, for a PMASR machine. Let us observe that, for $\alpha = 0$, the optimal δ_0 angle equals $\pi/4$. In other words, for a simple SyR motor (as well as for an Induction motor) the optimum flux locus at high speed is represented by the bisecting line. As the magnet contribution is increased, δ_0 is decreased.

$$\sin\delta_0 = \frac{1}{4}\big(-\alpha + \sqrt{\alpha^2 + 8}\big) \quad (6)$$

Fig.2 shows the vector diagram of a realistic situation at high speed, where λ_m is a little larger than λ, which represents in this case the minimum flux amplitude λ_{min}.

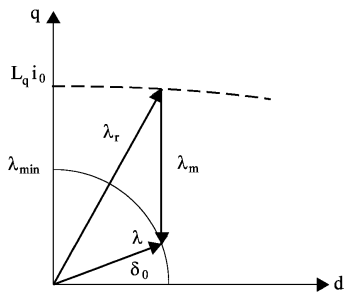

Fig. 2. Optimal vector diagram at maximum speed, for $\alpha \simeq 1.2$.

Since $\zeta >> 1$, the dotted (elliptic) curve is practically horizontal and eq.(7) is approximately valid, as defining the maximum i_0 current which is compatible with the λ_{min} constraint.

$$\frac{L_q\, i_0}{\lambda_{min}} \simeq \sin\delta_0 + \frac{\lambda_m}{\lambda_{min}} \quad (7)$$

Let us observe, from eq.(7) and Fig.2, that the ratio $L_q\, i_0/\lambda_{min}$ is near to 2, while for a simple SyR motor it would be $1/\sqrt{2}$, as said before. In practice, the added λ_m flux has increased the i_0 current by a factor near to 2.8, with respect to the basic SyR motor. A similar comparison would be carried-out with an equivalent induction motor: however, the lower q-axis inductance (σL_s) should be taken into account.

In conclusion, once the accepted λ_m/λ_{min} ratio is fixed, eq.(7) gives the minimum flux and consequently the CPSR once the rated flux is fixed. At fixed current, the lower L_q is, the lower the λ_{min} can be. In other words, the quantity of magnet flux λ_m is chosen at maximum speed, which represents the most critical situation: the behaviour at base speed will follow.

III. BASIC RELUCTANCE STRUCTURE

As seen, the maximum CPSR is reached through minimization of the L_q inductance that means maximizing rotor anisotropy, when L_d can be considered fixed. This argument has been thoroughly treated by former papers [3], [9]. Only a short synthesis will be given here, in order to introduce the following analysis.

With reference to an ideally slotless stator, two L_q components exist: that related to the flux circulating across the end of a rotor iron segment (L_{cq}) and that related to the flux flowing through the rotor and crossing the various flux barriers among segments (L_{fq}). It can be shown that L_{cq}/L_{md} (8) only depends on the number of flux-barriers and rapidly decreases as this number is increased. In practice, a three-barrier-per-pole structure is sufficient to make L_{cq} sufficiently low. On the contrary, L_{fq} is practically independent of the barrier number, while it mainly depends on the total insulation length, which in turn depends on stator design and the chosen airgap flux density value.

Calculation of L_{fq}/L_{md} can be made through the per-unit equivalent circuit shown in Fig.3, where f_k is the average value of the p.u. q-axis mmf (sinusoidal) over the segment span at the airgap and r_k is the resulting magnetic potential of the segment. The p.u. permeances are defined in the figure, while the base flux is $\mu_0\, A_q\, l$, being A_q the peak q-axis mmf and l the axial length.

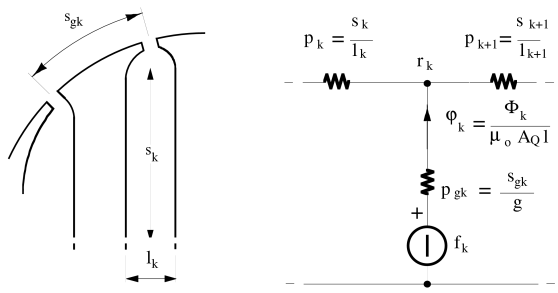

Fig. 3. p.u. equivalent circuit of the kth segment.

$$\frac{L_{cq}}{L_{md}} = 1 - \frac{4}{\pi}\sum_k f_k^2 \Delta\xi_k \quad (8)$$

$$\frac{L_{fq}}{L_{md}} = \frac{4}{\pi}\sum_k f_k\big(f_k - r_k\big)\Delta\xi_k = \frac{4}{\pi}p\frac{g}{r}\sum_k f_k\,\varphi_k \quad (9)$$

Eqs.(8) and (9) are valid, with $\Delta\xi_k = p\, s_{gk}/r$, where r is the rotor radius, g the airgap length. $[f_k]$ represent a sinusoidal-like distribution, because of the f_k definition. A proper design goal can be imposing that $[r_k]$ distribution has the same shape as $[f_k]$. In this way, also the p.u. fluxes $[\varphi_k]$ will be sinusoidal-like and the harmonic content is minimized. By posing $r_k = m\, f_k$, with $m < 1$, eq.(10) is written, from the equivalent circuit of Fig.3. By considering all the nodes, the system (11) is then obtained. Eq.(11) gives the wanted permeance distribution $[p_k]$, once m satisfies the geometrical constraint: allowed room across q-axis $l_a = \sum_k l_k$.

$$m\big(f_k - f_{k-1}\big)p_k + m\big(f_k - f_{k+1}\big)p_{k+1} = \big(1-m\big)f_k p_{gk} \quad (10)$$

$$[F][p_k] = \frac{1-m}{m}[p_{gk} \cdot f_k] \quad (11)$$

If the $[\Delta\xi_k]$ distribution is assumed to be uniform, $\Delta\xi_k = 2\pi/n_r = \textit{constant}$. In this case, also $p_k = \textit{constant}$ and the machine is complete, that is all the possible flux-barriers are present. The introduced spatial harmonics are of $(k\, n_r \pm 1)$ order only. More often, the rotors are incomplete (one or more barriers missing near q-axis). In this case, additional harmonics are present; however eq.(11) still gives the more convenient rotor design.

When a low-ripple design is wanted, care must be taken to properly choose the stator (n_s) and rotor (n_r) number of "slots" per pole pair, in order that the respective spatial harmonic $(h\, n_s \pm 1)$ and $(k\, n_r \pm 1)$ do not interact. $n_r = n_s \pm 4$ are quite often the best choices, as explained in [4].

IV. Rib and P.M. Design

The various iron segments of the ideal structure considered in the previous chapter must be connected to each-other by iron ribs, specifically designed to the centrifugal strength. These ribs are positioned at the rotor surface and also inside the rotor, depending on the mechanical needs. From the magnetic point of view the ribs represent a rotor leakage flux, which lowers torque and power factor. With reference to Fig.5, the ribs can be modelled by flux generators in parallel to p_k permeances (these in turn could be modified to take into account the permeability of the saturated rib iron).

If we consider now the PM inside each flux barrier, they can be modelled analogously to ribs, leading to the general p.u. equivalent circuit of Fig.5, while Fig.4 shows the schematic of the kth barrier and introduces new geometric variables, that approximately describe rib and magnet shapes. Note that s_k is an equivalent barrier lenght, to take into account the realistic shape.

In Fig.5, the parameters b_{res} and b_{sat} describe the magnet and rib properties, respectively. Let us point-out that magnet action counteracts the rib leakage. From Fig.5 eq.(12) is written. If $[r_k] = [f_k]$ is then posed, the $[\varphi_{mk}]$ distribution is derived wich zeroes the flux entering the various f_k generators. In this way, the PM flux exactly compensates for the L_{fq} inductance given by (9). In addition, the resulting $[\varphi_{mk}]$ distribution is sinusoidal-like, as the former $[\varphi_k]$ distribution

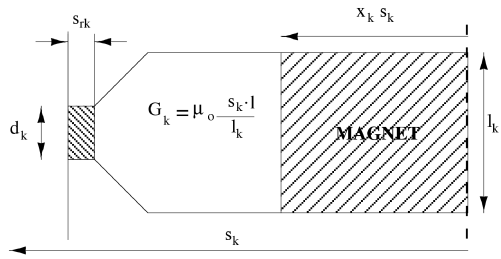

Fig. 4. Schematic of the k-th barrier, including rib and P.M.

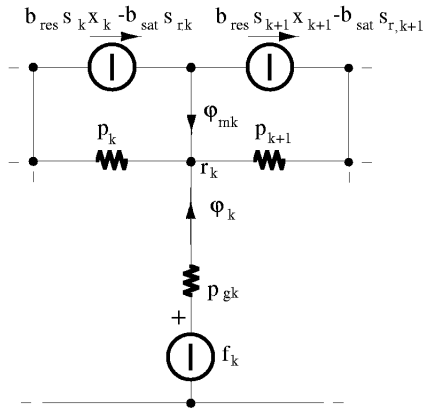

Fig. 5. P.u. equivalent circuit, of the kth barrier, with rib and P.M.

was, since coming from $[p_k]$ satisfying eq.(11). In this way the harmonic effect is minimized and torque ripple too.

$$p_k\big(r_k - r_{k-1}\big) + p_{k+1}\big(r_k - r_{k+1}\big) = p_{gk}\big(f_k - r_k\big) + \varphi_{mk} \quad (12)$$

$$\frac{L'_q}{L_{fq}}\varphi_{mk} = b_{res}\big(x_k s_k - x_{k+1}s_{k+1}\big) - b_{sat}\big(s_{rk} - s_{r,k+1}\big) \quad (13)$$

In general, the wanted magnet flux λ_m can be different from $L_{fq}\, i_0$, as shown in Fig.2. If $\lambda_m = L'_q\, i_0$ is posed, eq.(13) is simply obtained, as relating the needed $x_k\,, x_{k+1}$ parameters. From (13), a linear system of equations is written, whose solution gives the unknown vector $[x_k]$ that is the PM widths, since the PM lengths $[l_k]$ are supposed to be known from the former design step. Of course, an iterative process is required, since b_{sat} depends on the working point and the rib lengths $[d_k]$ are still to be designed. These lengths also influence the barrier permeabilities $[p_k]$.

V. Magnet Minimization

Following eq.(13) and the barrier scheme in Fig.4 a first amount of magnet is defined. A reduction in the magnet area can be then obtained if the PM dimensions $[l_k]$ are changed. Obviously, if the magnet depth is reduced the iron one has to be increased accordingly, as shown in Fig.6

This modification of the magnets area leads to modification of the permeances $[p_k]$, which implies modification of L_{fq}. However, the same flux φ_{mk} and the same distribution $[r_k]$

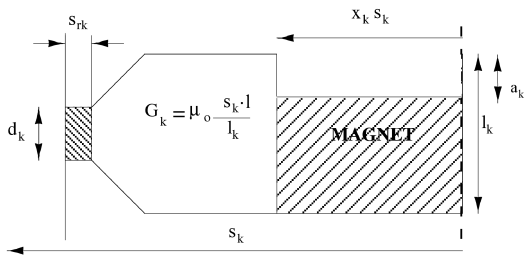

Fig. 6. Schematic of the k-th barrier with rib and modified P.M.

can be obtained, with different $[x_k]$ lenghts but less magnet area. The $[p_k]$ permeances are now the sum of the part outside the magnet $(1-x_k)s_k$ and the one inside the magnet $s_k\,x_k$, whose values vary as a functions of the ratio $y_k = a_k/l_k$. All calculations can be expressed with reference to the same equivalent circuit of Fig.5. Magnet areas as a function of the ratio y_k are expressed by eq.(14), while the element $C_{k,1}, C_{k,2}, C_{k,3}$ are defined in eq.s(15÷16), where μ_m and μ_{rk} are the relative permeabilities of PM and ribs, respectively.

$$S_k = s_k x_k \cdot (l_k - a_k) = \frac{C_{k,1} \cdot y_k^2}{C_{k,2} \cdot y_k - (1 - C_{k,3})} \tag{14}$$

$$C_{k,1} = (s_k - s_{rk})\,\mu_m\,l_k \quad C_{k,2} = (b_{res} \cdot l_k + 1) \tag{15}$$

$$C_{k,3} = \frac{s_{rk}}{s_k} l_k \left(\frac{\mu_{rk}}{d_k} + b_{sat} \right) \tag{16}$$

It can be shown that the area S_k in eq.(14) has a minimum with y_k and that this minimum exists in the range $0 < y_{k,opt} < 1$. This minimum is given by eq.(17).

$$y_{k,opt} = \frac{2 \cdot (1 + C_{k,3})}{C_{k,2}} \tag{17}$$

The eq.(17) points-out the possible reduction of the magnet area (cost) by modification of the permeance structure.

In a standard 4-pole rotor the barrier width is tipically larger at the barrier centre. Thus a barrier shape like that of Fig.4 can be easily implemented. Alternatively, the magnets should be split and shifted towards the barrier ends, where the barrier shows a lower width.

This second choice has two drawbacks: first, the new position implies that the magnets are two for each barrier, which should increase the manifacturing cost. Second, even if the magnet area is reduced, the new position is far from optimized, from the mechanical point of view. Anyway, some projects may take advantage from this possibility: it mainly depends on the mechanical design.

VI. MACHINE DESIGN

In the previous chapter only the rotor was analysed, while some main design choices where considered to be fixed. They are the pole-pair p the air-gap flux density B_g and the rotor radius r. B_g and r together define the main flux value. Let us consider here some design hints, in order to point-out the effect of the above mentioned parameters on the obtainable CPSR, as previously introduced.

In Fig.2 a limit current i_0 was defined, depending on U.G.O. performance and Lq value. If this current is equal to the current at base speed, a natural CPSR (NCPSR) is defined, which does not require any inverter oversizing. On the contrary, when the wanted CPRS is larger than the natural one, a larger current at base speed should be used and consequently the inverter is oversized.

As shown in Fig.7, at a fixed current amplitude and disregarding magnetic saturation, the flux vector λ_r moves on an elliptic locus, while the total flux $\lambda = \lambda_r + \lambda_m$ is shifted downwards. The better the anisotropy is the larger the main axis of the ellipse is. Of course, magnetic saturation limits the flux module at base speed.

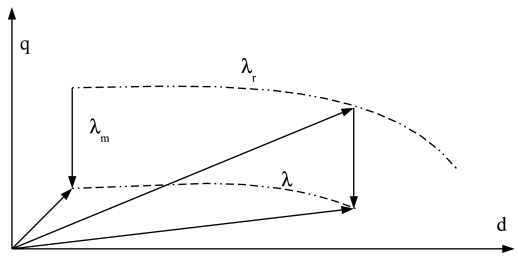

Fig. 7. Flux locus during flux-weakening, at constant current amplitude

The NCPSR, as defined above, comes from the ratio of maximum to minimum λ amplitudes, at constant voltage. To improve this, from the machine design point of view, the d-axis flux should be designed as large as possible without increasing the q-axis one. At fixed p and outer machine dimensions, a flux increase could be done by increasing both B_g and r. Consequently, the copper area is decreased and the mmf is decreased too. The torque is maintained, as a trade-off between flux and mmf, at least till too a little area is left to copper or the magnetizing needs become excessive.

When B_g is pushed up the teeth become larger and the barrier widths $[l_k]$ decrease, at constant barrier lengths $[s_k]$. Thus the p.u. permeances $[p_k]$ increase, together with L_{fq} inductance. Moreover, the slot leakege inductance $L_{\sigma s}$ increases too and the net effect on the $\lambda_{rq}/\lambda_{rd}$ ratio is poor, even if the resulting lower q-axis mmf is taken into account.

On the other hand, when the rotor radius is increased, $[p_k]$ could be maintained constant, together with L_{fq}. In addition $L_{\sigma s}$ is lowered, in this case. As a consequence the best approach to increase the main flux is to increase r, while maintaining B_g at reasonably standard values.

Both strategies reduce the copper amount but generally increas that of PM material. A cost trade-off may be found. However, the PM amount should be minimized as illustrated in the previous chapter.

Let us now consider the choice of the pole-pair. It heavily affects the anisotropy ζ and the NCPSR, as a consequence. To highlight this the various contributions to the q-axis inductance can be evidenced. The L_{cq}/L_{md} ratio (8) does not depend on p while L_{fq}/L_{md} does, as shown by (9). Also $\sum_k f_k \varphi_k$ could depend on p, but this dependence can be neglected, as a first

approximation, since the $[p_k]$ permeances in Fig.3 can be made quite insensitive to p. Moreover, the slot leakege inductance $L_{\sigma s}$ can be written as (18), where p_s is the p.u. slot permeance which, in turn, is nearly proportional to p, at fixed rotor radius.

$$\frac{L_{\sigma s}}{L_{md}} = 2\,\pi\,p\,\frac{g}{r}\,\frac{p_s}{n_s} \tag{18}$$

As seen, both L_{fq} and $L_{\sigma s}$ increase with p and consequently ζ is rapidly lowered, as p is increased.

A further contribution to the L_{rq} flux is given by rotor rib leakage, in SyR motors. Rib leakage depends on rib widths $[s_{rk}]$, which depend on geometry and maximum speed.

If p is increased, at fixed r and speed, the segment weight can be made decreasing as p^{-2} while the d-axis flux only decreases as p^{-1}. Thus the rib leakage would be reduced as p^{-1}. However, large p values generally require large rotor diameters, also to reduce the slot leakage (18). As a consequence the rib widths must be increased to limit the specific mechanical stress. On the other hand, also the rotor speed is typically reduced with p. We can than conclude that the rib leakage does not represent a critical point in general, while it could be for some specific high speed application. Also, let us point-out that rib leakage is compensated by some PM flux, in a IPM-PMASR motor. This PM flux is not linked to stator windings and does not contribute to U.G.O., which represents the main limit to the NCPSR, as seen before (7).

In conclusion incresing the number of poles generally reduces the NCPSR, because the d-axis flux is reduced while the q-axis one is maintained (L_{fq}) or even increased ($L_{\sigma s}$), except that rotor radius is properly increased. As a consequence, $p = 2, 3$ appears to be the best choices in general, also depending of the machine size. Of course other p values could be suggested in case of particular constraints (e.g. a ring shaped machine).

Last, still regarding machine design, the iron loss due to slot harmonics has to be mentioned, as a possible drawback of the IPM-PMASR machine, when a large CPSR is set. This point is well beyond the paper aim. Suffice it to say that the n_s, n_r numbers must be accurately chosen also with reference to this possible problem.

VII. PRACTICAL DESIGNS

We analyze here two existing motors, to give a better illustration of the above presented analysis.

The first motor is shown in Fig.8 and represents a quite small machine, 4-pole, rated 3Nm @ 4.5A peak. Its outer diameter is 110mm, 50mm the stack lenght. The rotor design speed is 20000rpm. In Fig.9 the measured flux-current characteristics are shown, while Fig.10 reports the maximum Nm/A curve. The rated point R is $i_d = 2.9$ and $i_q = 3.5$. From Fig.9 the correspondig flux linkages are found ($\lambda_d \simeq 0.27$, $\lambda_q \simeq -0.01$). The flux amplitude of ~ 0.27 leads to a base speed of $\sim$ 3300rpm, when a DC-bus voltage of 350V is provided. From Fig.9 the P.M. flux at no load is $\lambda_m \simeq 0.07$ (temperature variation disregarded). The unsaturated anisotropy ratio ζ is ~ 7. If $\lambda_m/\lambda_{min} = 1.2$ is supposed, from (5) $\alpha = 1.4$ is found, leading to $\sin\delta_0 = 0.44$. From (7), with $\lambda_{min} = 0.058$, $L_q i_0 = 0.095$ results. Being $L_q \simeq 17mH$, the limit current $i_0 = 5.6$ is found.

Since the limit current at high speed is larger than the rated one, the P.M. quantity is larger than required. A 20% less λ_m ($\simeq 0.046$) would have led to a NCPSR of $0.27/0.046 = 5.9$. Instead, we have a CPSR= 4.7 or alternatively, we must accept a λ_m/λ_{min} larger than the set value. On the other hand, if the machine is overloaded to 5.6A @ 4Nm, the actual P.M. compensation becomes correct., with a NCPSR of $0.29/0.058 = 5$. Of course, the more the motor is loaded, the lower the NCPSR is.

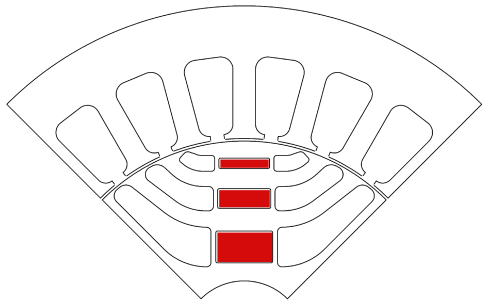

Fig. 8. 4-pole machine (small and fast)

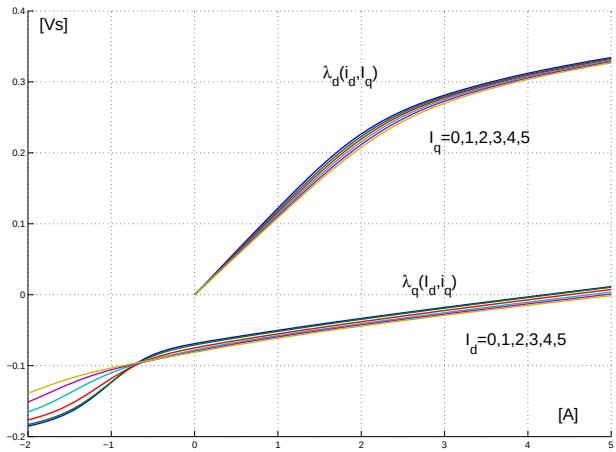

Fig. 9. Magnetic characteristics of the 4-pole machine

Let us now pass to a completely different motor, much larger but also constrained to a ring shaped room (mild-hybrid application). The motor lamination is shown in Fig.11. Outer diameter is 284mm, stack lenght is 55mm. The motor is 12-pole, designed up to 9500rpm; rated torque is 70Nm @ 220A peak. In Figs. 12 and 13 the flux-current behaviour and the max Nm/A locus are shown. From max Nm/A locus the point $i_d = 137$, $i_q = 160$ is evidenced (70Nm), leading to $\lambda_d = 0.049$, $\lambda_q = 0.001$. The current and flux amplitudes are $210A$ peak and $0.049Vs$. From Fig.12 $L_q = 0.125mH$ and $L_d = 0.65mH$ (initial), giving to $\zeta = 5.2$. Thus, from (5),(6),and (7), assumed $\lambda_m/\lambda_{min} = 1.2$, $\alpha = 1.49$, $\sin\delta_0 = 0.43$, $L_q i_0/\lambda_{min} = 1.63$ are obtained. Since $\lambda_m = 0.02$ (Fig.12) we get $i_0 = 209$. In this case the limit current equals the rated one and the machine is well compensated. The resulting NCSPR is $0.49/0.02 \simeq 3$. The base speed is 2000rpm, thus

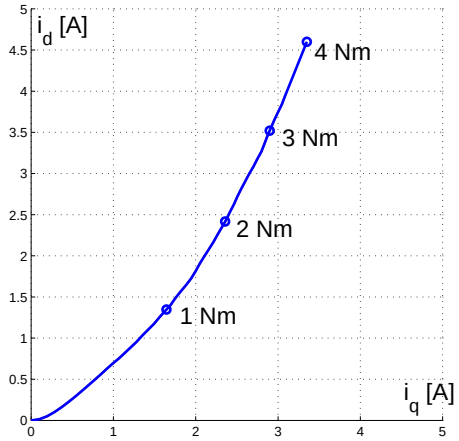

Fig. 10. 4-pole machine. Maximum Nm/A locus on the $i_d\, i_q$ plane

the maximum one would be 6000rpm. In practice, a bit larger CPSR (2000÷6500rpm)is reached, since the voltage at base speed is slyghtly lower than that at high speed. Of course, this results in some (small) inverter oversizing. In conclusion, this machine still gives a good CPSR performance, in spite of the large pole number and the resulting low anisotropy.

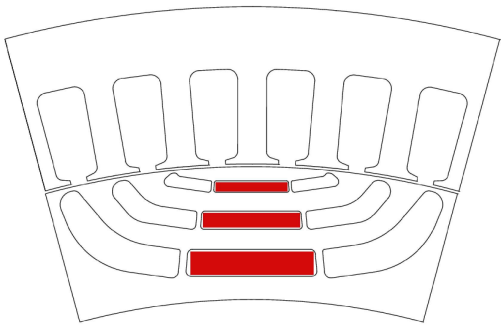

Fig. 11. 12-pole machine (big and fast)

VIII. CONCLUSIONS

An IPM machine suited fo large CPSRs must have a PMASR structure, that is a very good anisotropic rotor. This is obtained through a multiple barrier structure, whose shape must be accurately designed, also in order to minimize the amount of P.M. material. The cross-saturation effect is present, although reduced by the effect of P.M. compensation. Care must be taken to avoid additional losses in the iron at high speed, due to slot harmonics.

In conclusion, if properly designed, the IPM-PMASR machine can get superior performance when a large CPSR is needed, superior to that reachable by a well designed Induction Machine.

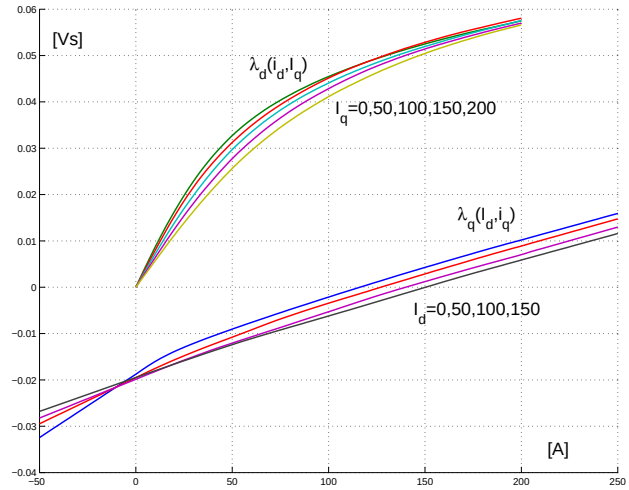

Fig. 12. 12-pole amchine. Magnetic characteristics

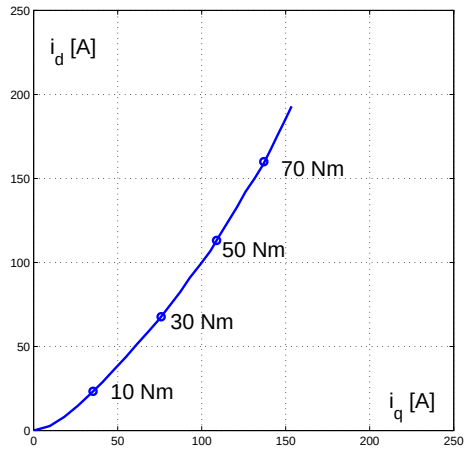

Fig. 13. 12-pole machine. Maximum kT locus on the IdIq plane

REFERENCES

[1] R.Schiferl and T.A.Lipo,"Power capability of salient pole P.M.synchronous motors in variable speed drives" *IEEE-IAS annual meeting 1988*,pp.23-31.

[2] Fratta A., Vagati A., Villata F.: "Design criteria of an IPM machine suitable for field-weakened operation", *ICEM 90 Conference*, Boston, USA, 13-15 August 1990, pp. 1059-1065.

[3] A.Vagati, I.Marongiu, G.Franceschini, G.P.Troglia, "Design criteria of high performance synchronous reluctance motors", *Conf. Record. of IEEE-IAS annual meeting 1992*, 4-9 Oct.1992, Vol.1, pp:66-73

[4] A. Vagati, M. Pastorelli, G. Francheschini, S.C. Petrache, "Design of low-torque-ripple synchronous reluctance motors" *IEEE-IA Transactions on* Vol 34, Issue 4, July-Aug. 1998 pp:758-765

[5] A.Vagati, M.Pastorelli, G.Franceschini, F.Scapino, "Impact of cross saturation in synchronous reluctance motors of the transverse-laminated type", *IEEE Trans. on Industry Applications*,Vol.36, Issue:4, July-Aug.2000 pp:1039-1046

[6] E.C. Lovelace, T.M. Jahns, J.H. Lang, "A saturating lumped-parameter model for an interior PM synchronous machine", *IEEE Trans Industry Application*, Vol.38, pp.645-650, May-June 2002.

[7] Boldea, I. Tutelea, L.Pitic,. "PM-assisted reluctance synchronous motor/generator (PM-RSM) for mild hybrid vehicles: electromagnetic design", *IEEE Trans. on Industry Applications*, Vol.40, Issue:2, March-April 2004 pp:492 - 498

[8] Sibande, S.E.; Kamper, M.J.; Wang, R.; Rakgati, E.T. "Optimal design of a PM-assisted rotor of a 110 kW reluctance synchronous machine" *AFRICON, 2004. 7th AFRICON Conference in Africa* Vol 2, 2004 pp:793-797

[9] A.Vagati, P.Guglielmi, "Design, Analysis, and Control of IPM Sinchronous Machines" *Tutorial Course Notes at IEEE-IAS 04 Meeting.*, Chapter 6, CLEUP Padova Italy, ISBN 88-7178-898-2.

[10] Seok-Hee Han; Jahns, T.M.; Aydin, M.; Guven, M.K.; Soong, W.L. "Impact of Maximum Back-EMF Limits on the Performance Characteristics of Interior Permanent Magnet Synchronous Machines" *2006 IEEE 41 IAS Annual Meeting* Vol 4, Oct. 2006 pp:1962-1969